

GALEX, Optical and IR Light Curves of MQ Dra: UV Excesses at Low Accretion Rates

Paula Szkody¹, Albert P. Linnell¹, Ryan K. Campbell², Richard M. Plotkin¹, Thomas E. Harrison², Jon Holtzman², Mark Seibert³, Steve B. Howell⁴

ABSTRACT

Ultraviolet light curves constructed from NUV and FUV detectors on *GALEX* reveal large amplitude variations during the orbital period of the Low Accretion Rate Polar MQ Dra (SDSSJ1553+55). This unexpected variation from a UV source is similar to that seen and discussed in the Polar EF Eri during its low state of accretion, even though the accretion rate in MQ Dra is an order of magnitude lower than even the low state of EF Eri. The similarity in phasing of the UV and optical light curves in MQ Dra imply a similar location for the source of light. We explore the possibilities of hot spots and cyclotron emission with simple models fit to the UV, optical and IR light curves of MQ Dra. To match the *GALEX* light curves with a single temperature circular hot spot requires different sizes of spots for the NUV and FUV, while a cyclotron model that can produce the optical harmonics with a magnetic field near 60 MG requires multipoles with fields > 200 MG to match the UV fluxes.

Subject headings: binaries: close — novae, cataclysmic variables — stars: individual (MQ Dra, EF Eri) — ultraviolet:stars — white dwarfs

1. Introduction

The cataclysmic variable MQ Dra was discovered in the Sloan Digital Sky Survey as SDSSJ155331.12+551614.5 (Szkody et al. 2003; S03). Its peculiar optical spectrum showed

¹Department of Astronomy, University of Washington, Box 351580, Seattle, WA 98195, szkody@astro.washington.edu, plotkin@astro.washington.edu, linnell@astro.washington.edu

²Department of Astronomy, New Mexico State University, Box 30001, MSC 4500, Las Cruces, NM 88003, cryan@nmsu.edu, tharriso@nmsu.edu, holtz@nmsu.edu

³Observatories Carnegie Institute of Washington, 813 Santa Barbara St., Pasadena CA 91101, mseibert@ociw.edu

⁴National Optical Astronomy Observatories, 950 N. Cherry Avenue, Tucson, AZ 85726, howell@noao.edu

narrow, highly polarized cyclotron emission features that could be explained with an origin from a white dwarf with a magnetic field near 60 MG. These features underwent large periodic changes during time-resolved photometric and spectroscopic observations, providing an orbital period of 4.39 hrs. Aside from the cyclotron features, the red portion of the spectrum revealed TiO bands, indicating an M4-M5V secondary star whose brightness provides a system distance of 130-180 pc (S03, Schmidt et al. 2005; S05, Harrison et al. 2005). Modeling the continuum after subtraction of the secondary indicated a cool white dwarf $<10,000\text{K}$, but the flux at the blue end of the spectrum was larger than from a white dwarf alone, suggesting an additional hot spot (S05). X-ray observations (Szkody et al. 2004) also hinted at an upturn at soft energies, possibly indicating a hot component. Both the appearance of the cyclotron features and the X-ray fluxes were consistent with a cool plasma ($kT \sim 1\text{ keV}$) and extremely low accretion rate ($10^{-14}M_{\odot}\text{ yr}^{-1}$). The exceptionally low accretion rates in these types of systems resulted in the identification of a new category of magnetic cataclysmic variables called Low Accretion Rate Polars (LARPs; Schwöpe et al. 2002). The fact that MQ Dra has a relatively long orbital period and a very cool white dwarf led to the speculation that this could be a system which is a pre-Polar i.e. the white dwarf has never been heated by any active accretion and the cyclotron radiation is provided only by wind accretion from the secondary. In contrast, a Polar has known states of active accretion via a mass transfer stream from the secondary.

This interpretation is complicated by the fact that most Polars spend much of their lives in low states of accretion (Ramsay et al. 2004; Araujo-Betancor et al. 2005) that can reach low accretion rate values near those for LARPs. Active accretion episodes could produce heated areas that remain hot for long periods of time after the accretion has stopped. This is borne out by UV studies of systems during low states (Araujo-Betancor et al. 2005; Gänsicke et al. 2006) where 30,000-70,000K hot spots on the white dwarfs during low states were needed to match the observed fluxes. A *GALEX* study of the Polar EF Eri four years after it entered a low state (Szkody et al. 2006; S06) showed a 20,000K spot was needed on a 9500K white dwarf to come close to producing the large amplitude modulations visible in the UV light curves. However, simple black bodies for the white dwarf and spots could not reproduce both the amplitude of the modulations and the spectral energy distributions. Schwöpe et al. (2007; Sw07) had better success with the spectral energy distribution using actual white dwarf models but they did not show UV light curves with which to compare UV observations. Since the white dwarfs in known active Polars observed during low states are generally hotter than those found in LARPS, the influence of the active accretion episodes is not clear. To obtain further insight into the heating of the white dwarf in LARPS, we undertook *GALEX* observations of MQ Dra, which has a cooler white dwarf with a higher magnetic field compared to the white dwarf in EF Eri, and an accretion rate that is even

lower than EF Eri during its lengthy low state.

2. Observations

The *GALEX* satellite obtains images with a FUV detector (1350-1750Å) and a NUV detector (1750-2800Å) (Martin et al. 2005). MQ Dra was observed during two intervals, one in June 2005 and the other in July 2006. The first set of observations was done when the FUV detector was not operational, while both detectors were used in 2006. The times of observation are listed in Table 1. Calibrated images in 240s intervals were generated from the observations, phased according to the ephemeris below and then magnitudes inside a 9 pixel radius aperture were measured with the IRAF¹ routine *qphot*. An annulus of 3 pixels around the aperture was used to obtain and subtract a background. The magnitudes were converted to flux from the values given in the *GALEX* online documentation² (FUV $m_0=18.82=1.40\times 10^{-15}$ ergs $\text{cm}^{-2} \text{s}^{-1} \text{Å}^{-1}$ and NUV $m_0=20.08=2.06\times 10^{-16}$ ergs $\text{cm}^{-2} \text{s}^{-1} \text{Å}^{-1}$).

Since the previous available ephemeris determined from 5 nights of observations (S03) was not sufficient to phase the *GALEX* data to a cyclotron or geometric phasing, we obtained further optical data during 22 nights in the interval from 2007 Feb 25 - May 4. These data were obtained on the NMSU 1m telescope at Apache Point Observatory, using a CCD and *BVRI* filters with integration times of 90, 60, 60, 60s respectively. Differential light curves were constructed using nearby stars on the same frames and calibrated with the magnitudes for the comparison stars that were used in S03.

As shown by the phase resolved spectra in S03 and S05, the optical light curves of MQ Dra are dominated by the prominent cyclotron peaks at 4600, 6200 and 9200Å, which come into the *BVRI* bandpasses. Since these harmonics change amplitude due to the changing viewing angle of the cyclotron region during the orbit, a distinct sinusoidal variation is produced (S03). Although this is a broad feature, we could combine all the nights with good *R* filter coverage (16 nights) to obtain a better period using the IRAF routine *pdm*. The past spectroscopic and polarimetric data of S05 showed that the blue to red crossing of the H α emission line was close to the peak amplitude of the cyclotron harmonics. Since the H α emission had the same phasing and amplitude as the TiO bandheads, it allows a definition

¹IRAF (Image Reduction and Analysis Facility) is distributed by the National Optical Astronomy Observatories, which are operated by AURA, Inc., under cooperative agreement with the National Science Foundation.

²See <http://galexgi.gsfc.nasa.gov/tools/index.html>

of phase 0 as inferior conjunction of the secondary (and the peak of the R band light curve). Thus, we obtained the following ephemeris to phase the *GALEX* data:

$$\text{phase 0} = \text{HJD } 2,454,156.9138 + 0.182985 \pm 0.000005\text{E}$$

Since the NUV light curves from 2005 and 2006 were similar, this phasing allowed us to combine the 2005 and 2006 NUV datasets to maximize the S/N.

Infrared photometry of MQ Dra was also obtained on the KPNO 2.1 m telescope with the Simultaneous Quad Infrared Imaging Device (SQIID)³, which obtains JHK images simultaneously. Data were obtained on two consecutive nights, 2007 May 28 and 29. On 28 May, the first exposure began at 03:42:01 UT and data were obtained over the next 3.3 hrs, while on May 29 the observations started at 03:31:57 and continued for the next 2.7 hrs. The images were reduced with standard procedures, then differential photometry was performed with respect to several field stars. The differential magnitudes were then corrected to absolute JHK photometry using data from the 2MASS Point Source Catalog, and the data were phased with the above ephemeris.

3. MQ Dra Light Curves

The *GALEX* NUV and FUV light curves are shown in Figure 1, along with the phased $BVRI$ light curves from 2007. All the light curves have large variability, with peak-to-peak amplitudes of 0.7, 0.8, 0.5, 1.0, 0.9 and 0.2 mags for FUV, NUV, B , V , R , I respectively. The JHK light curves are shown in Figure 2. The K -band light curve of MQ Dra reveals classic ellipsoidal modulations with one minimum being slightly deeper than the other. This difference can be explained if the secondary star fills (or almost fills) its Roche lobe and is distorted so that the white dwarf-facing hemisphere (viewed at phase $\phi = 0.5$) is further from the center of the secondary star and therefore cooler. The H -band light also appears to be dominated by ellipsoidal variations, but a non-sinusoidal light source, presumably cyclotron emission, appears to contaminate the light curve. The J -band light curve is even more complex, and only seems to bear a small imprint of the ellipsoidal variations. The spectral type of the secondary star for MQ Dra was previously determined by S05 to be M5V. The K -band spectrum for this source (see Harrison et al. 2005), however, suggests a spectral type closer to M4V due to the depth of the Ca I triplet (at 2.26 μm). In the light curve modeling below, we assume that the secondary star is an M4V.

³See <http://www.noao.edu/kpno/sqiid/sqiidmanual.html>

The IR light curve modeling was accomplished with the Wilson-Divinney code WD2005⁴, which includes reflection effects. For the modeling, we assumed a white dwarf primary with $T_{\text{eff}} = 8,000$ K, an M4V secondary ($T_{\text{eff}} = 3,200$ K), and used the square root limb darkening coefficients from Claret (2000b), the gravity darkening value of 0.3 (Claret 2000a) and an albedo of 0.60 (Nordlund & Vaz 1990). The best fitting model for the K -band has an orbital inclination of $i = 35^\circ$, and is plotted in red in Figure 2. It is clear from this figure that the light from just the secondary star is inadequate to completely explain either the flux level or variations seen in the J and H -bands. Since cyclotron emission from the $n = 1$ (at $1.8 \mu\text{m}$) and $n = 2$ (at $0.9 \mu\text{m}$) harmonics from a $B = 59$ MG field is expected to be present in both the J and H -bands, this emission likely creates the observed discrepancy between the model and observed light curves. The value for the inclination derived assuming a contact binary is much lower than that preferred by the cyclotron modeling ($i = 60^\circ$, see section 6). If the assumption of a contact binary is relaxed, the infrared light curves can be modeled with larger orbital inclinations. To investigate this possibility, we ran WD2005 in non-contact binary mode, but starting with a model where the secondary star essentially filled its Roche lobe (“ R_{contact} ”), and using stellar parameters that allowed us to reproduce the light curves found for the contact case with $i=35^\circ$. We then proceeded to shrink the radius of the secondary to create light curves for a system that is further and further from contact. We were able to create models where the light curves are well modeled using higher orbital inclinations. The results are listed in Table 2. Note, however, that in this mode, the differences in the observed minima in the model light curves are so small as to be undetectable given the error bars on our photometry. This is true even for the 94% radius case. But the observed minima *do* differ. It is unclear whether this is a deficiency in the light curve modeling program, or not, but further investigation will require stronger constraints on the masses of the two components as well as a better estimate of the temperature of the white dwarf.

The optical light curves are similar in amplitude and appearance to those shown in S03 (which used arbitrary phasing), while the increased coverage in 2007 allows for a better resolution of the features. In particular, the double-humped structure in the B light curve is confirmed. S03 had speculated this could be the result of cyclotron beaming with a grazing eclipse of the accretion area at the lowest dip (phase 0.55 in Figure 1). It is intriguing that there is a slight dip in the FUV light curve near phase 0.05 (which is near the secondary minimum in B) but the poor time resolution of the FUV and the large error bar on this single point does not permit any conclusive link.

As in EF Eri (S06), the UV light curves of MQ Dra show a prominent sinusoidal mod-

⁴WD2005 is an updated version of WD98, and can be obtained at this website maintained by J. Kallrath: <http://josef-kallrath.orlando.co.nz/HOMEPAGE/wd2002.htm>

ulation, with the peak UV flux close to the peak cyclotron times, thus strongly suggesting a link between the UV and cyclotron sources (the magnetic pole area). The amplitude of the modulation in the FUV in MQ Dra is comparable to that in EF Eri, while the NUV amplitude in MQ Dra is even larger than its FUV and about three times larger than the NUV of EF Eri. While EF Eri and MQ Dra are known to have very different field strengths (13 vs 60 MG) and white dwarf temperatures (9500K vs 8000K), it is obvious that a single temperature white dwarf (i.e. as evidenced by a constant UV light curve) cannot explain the observed light curves in either system.

Two possible explanations come to mind: 1) there is a hot spot on the white dwarf near the magnetic pole causing the UV modulation, as used by Araujo-Betancor et al. (2005) to model the UV fluxes of low state Polars and by Gänsicke et al. (2006) to model the UV light curves of AM Her or 2) the UV modulation is caused by phase dependent cyclotron harmonics as is known to be the cause of the optical variability. We explore these two options with simple models below.

4. MQ Dra Spot Model

To determine the feasibility of a hot spot, we used the BINSYN modeling code (Linnell & Hubeny 1996) to calculate synthetic light curves and spectra of MQ Dra. The model code calculates the SED of a white dwarf using TLUSTY (Hubeny 1988) and SYNSPEC (Hubeny, Lanz & Jeffery 1994). The TLUSTY model uses a specified mass and radius (producing an associated $\log g$) and SYNSPEC produces continuum spectra plus absorption lines of H and He. To minimize the free parameters, we used the simplest approximations of a circular, isothermal hot spot to produce the light variation. Recognizing that satisfactory models for radiation transfer in the presence of a strong magnetic field are not available (Wickramasinghe & Ferrario 2000), we used white dwarf SEDs to represent the spot. The BINSYN modeling code was then used to assign spot T_{eff} , latitude, longitude and angular radius and, for a given parameter set, to calculate a series of synthetic system spectra that included contributions from the white dwarf, the spot, and the secondary star. The code then integrated, for each synthetic system spectrum, the products of the FUV, NUV and optical passbands and the synthetic system spectrum. The resulting calculated synthetic light curves were then compared with the observed light curves. In our model, a key element in producing the light variation with orbital phase is the variable foreshortening and limb darkening of the spot as the white dwarf rotates. It is important to note, in the comparison with the observations, that neither the FUV nor NUV observed light curves are perfect sinusoids.

Previous estimates of the white dwarf temperature (obtained by subtracting the secondary and cyclotron harmonics and fitting white dwarf fluxes; S03, S05, Ferrario et al. poster at IAU Coll. 190, unpublished) obtained temperatures from 6000-8000K with an upper limit of 10,000K. Our model uses a temperature of 8000K. Since the Ferrario et al. model and our cyclotron modeling preferred inclinations near 60° , and our *JHK* light curve modeling set a minimum inclination of 35° , we constructed models using these two limits.

Our search for a simple spot model to simulate both the FUV and NUV light variation of MQ Dra was unsuccessful in that the observed light variation cannot be simulated by our model employing a single, isothermal, circular spot which does not extend beyond the pole. The challenge is the approximately equal light amplitudes in FUV and NUV. Many combinations of spot parameters can simulate either light curve individually. Table 3 lists one pair of models for each inclination with the corresponding light curves shown in Figure 3. For $i=60^\circ$, the maximum spot angular radius is 15° to avoid extending beyond the pole; in this case the spot center is at a latitude of 75° . The lower inclination (35°) produces similar results.

We simulated the NUV light curve first, and the final parameters required a spot radius close to the limiting value. The adopted T_{eff} would not produce the observed light amplitude for a smaller spot. An appreciably larger T_{eff} would have exacerbated the difference in FUV and NUV synthetic light amplitudes for a given common spot size. The FUV spot angular radius was determined after the spot T_{eff} had been determined, and was adjusted to produce a synthetic FUV light amplitude matching the observed amplitude. Note how much smaller the FUV spot radius is, as compared with the NUV spot radius. While a smaller FUV spot is reasonable if there is a temperature stratification, i.e. a small hot area surrounded by a larger cool area, we felt we did not have enough constraints within our limited data to further increase the number of free parameters.

We also extended the model fits to the optical region. As expected, the white dwarf and spot model produce synthetic light amplitudes much smaller than the amplitudes observed in B or V. This is not surprising as the optical spectra (S03,S05) show that the optical is dominated by the cyclotron harmonics, not a stellar continuum.

These spot models are purely empirical. There are several options that could lead to other solutions i.e. a non-isothermal spot with a smaller and hotter central region contributing the bulk of the FUV source as noted above, a non-circular or vertically extended spot, a source other than a spot (Section 6). Constraining these options will require better phase-resolved UV spectra to determine the source of the light.

5. EF Eri Spot Model

We also tried to model EF Eri with our latest spot model. Our original attempt to fit the GALEX data on EF Eri (S06) used the Wilson-Devinney code WD2005 which involves black body representations for both the white dwarf (9800K) and the spot (20,000K). Applying the better modeling technique described above for MQ Dra with the parameters of EF Eri (Table 4) resulted in a spot of 24,000K with a radius of 5.5° situated at a latitude of 60° . In this case, a single size spot can provide a reasonable match to the amplitudes of both the FUV and NUV light curves. The fits to the UV light curves are shown in Figure 4 while the contribution of the spot and white dwarf at the brightest phases of the lightcurve are shown in Figure 5. As found by Sw07, using actual white dwarf fluxes improves the match to the spectral energy distributions at maximum and minimum light, but Sw07 require a larger spot than our BINSYN model fits which use a hotter, smaller spot to produce the same amount of FUV flux. Table 5 compares the parameters of the two models. An important point is that while both models show that a spot model can represent the light variation, there are enough free parameters that multiple solutions are possible. A key difference between the Sw07 model and ours is that their spot encompasses the pole and depends on the disappearance of some of the spot below the horizon (self-eclipse) during part of an orbital cycle in order to produce the light variation. Although their model produces light variation, we note that the spot is large (half opening angle of 24°) and the required spot size depends on the adopted orbital inclination (Sw07 adopted 60° , while we used 45° based on the Harrison et al. (2003) analysis, and Campbell et al. (2008) found 55° from their cyclotron modeling). The Sw07 model would require an appreciably larger spot if $i=45^\circ$. As in MQ Dra, it is obvious that the shape of the UV light curves is not a perfect sinusoid, implying the hot spot is not a simple circular, isothermal spot.

6. MQ Dra Cyclotron Model

The cyclotron modeling was done using a Constant Lambda (CL) code first built by Schwobe et al. (1990), which uses four parameters: B (the magnetic field strength), kT (the plasma temperature), Θ (the viewing angle to the magnetic field), and $\log\Lambda$ (the “size-parameter” of the system, which is a proxy for column density). The optical data used are the time-resolved spectra from the Bok 2.3m that are shown in Figure 9 of S05.

To fit the models, we tried to keep the parameters as consistent with the Ferrario et al. cyclotron model results as possible, using $B = 60$ MG, $kT = 1$ keV, and $i = 60^\circ$ for initial constraints. Additionally, we used the fact that there is a small amount of motion ($\sim 120\text{\AA}$) in the $n = 3$ (6000\AA) harmonic to constrain the viewing angle. Interestingly, this cyclotron

hump appears reddest (implying the highest value of Θ) at the cyclotron minimum (phase 0.43). Coupled with the fact that the ratio of the $n = 3$ and $n = 4$ harmonics show the greatest parity at that phase, we conclude that the highest value for the viewing angle must occur at cyclotron minimum. We initially assumed that the orbitally averaged value of Θ would equal the system inclination, and that β (the angle between the rotation and magnetic axis) was the absolute angular deviation of the viewing angle, while $\log\Lambda$ was left as a free parameter. To match the observed spectra, the models were normalized to the data at $0.62 \mu\text{m}$. The phase-resolved cyclotron models are shown in Figure 6, with Table 6 listing the values of the model parameters for each spectrum. Roughly, the orbitally averaged values for the salient parameters are: $B = 59 \text{ MG}$, $kT = 1.8 \text{ keV}$, and $\log\Lambda = 3.8$. The derived geometry is consistent with a single spot $i = 68^\circ$, and $\beta = 7^\circ$.

While this cyclotron model does an excellent job at predicting the changing morphology of the visual spectrum, the observed fluxes are difficult to reconcile because for the derived geometry, the spot remains continuously visible. With these parameters, our models suggest that the maximum amount of flux from the cyclotron emission region should occur at $\phi = 0.43$, but this is near where the observed *minimum* occurs. Given that the $n = 3$ and $n = 4$ harmonics have nearly identical fluxes, and are reddest at this phase, the viewing angle should be at a maximum, which in turn should produce the greatest amount of observed cyclotron emission. Comparing the raw, un-normalized model intensities to the photometry suggests that the fluxes at photometric minimum are down by a factor of six if we assume an equal emitting area at all times. We can explain this variation if we assume the values for i and β derived from the cyclotron modeling are incorrect, and that the accretion region is partially self-eclipsed.

For a simple geometry (a uniform, cylindrical column), we find that we can relate $i + \beta$ to the column height (h) through the following equation:

$$h = (1 + \eta)R_{\text{WD}}(\tan^2(i + \beta - 90) - 1.0)$$

where η is the fraction of the column that remains visible, and R_{WD} is the radius of the white dwarf. Assuming values of $0.01 \leq h \leq 0.05 R_{\text{WD}}$, we found values of $97.5^\circ \leq (i + \beta) \leq 106.5^\circ$, as listed in Table 7. The geometries implied by these combinations of i and β cannot reproduce the observed viewing angles without curvature of the field lines. Assuming a dipole field, Beuermann, Stella & Patterson (1987) show that the angle of curvature, b , is related to the magnetic colatitude by the equation $b = 3/2 \beta$. We used a root-finding scheme to find values of b for a range of orbital inclinations that reproduce the observed phase dependence of the viewing angle θ (see Fig. 7). The mean value for b is 68° , which implies $\langle \beta \rangle \sim 45^\circ$. This, in turn, restricts the orbital inclination to the values listed in Table 7. We believe that this is the simplest interpretation, but more complex field structures and/or accretion

regions could also reproduce the observations.

Finally, we attempted to fit the observed SED at both photometric minimum and maximum. In Figure 8, we show the observed photometry for these two phases, obtained from the GALEX, NMSU, and KPNO data for the UV, optical, and near IR, respectively. Using the color-magnitude table for pure hydrogen white dwarfs with $\log(g) = 8$ in Bergeron, Wesemael, and Beauchamp (1995) at 180 pc with $\lambda F_\lambda \simeq 20\%$ below the NUV photometry at photometric minimum implies $T \simeq 8400$ K. In this work, we adopt a slightly lower temperature of 8000 K. This WD (green line) is co-added with a M4 secondary normalized to the K-band photometry. In addition, we added our optical cyclotron models for both phases, finding that the SEDs were well reproduced in the IR and the optical, but that the noted UV photometric variability was still unexplained. Therefore, we added a second cyclotron model to explain the UV photometry. As in EF Eri (Campbell et al. 2008), it was difficult to constrain the UV cyclotron models without proper phase-resolved UV spectroscopy. We assumed that the UV cyclotron model has identical model parameters to the optical model, but with the magnetic field strength increased to push the harmonics into the UV. A magnetic field of $B = 235$ MG produced harmonics in the right places; this value was the lowest field strength which could be reasonably fit to the observed data. This high field strength is not unknown among Polars as AR UMa shows a similar value for B (Schmidt et al. 1996). To calibrate the fluxes, we assumed that the peak flux (in F_λ) of the $n = 3$ harmonics for both models were identical. The model spectrum was then integrated over the transmission function of the GALEX NUV and FUV bandpasses using the IRAF package CALCPHOT, and the synthetic photometric point compared to the GALEX photometry.

At photometric maximum, we found that while the NUV point was well predicted, the model could not produce enough flux in the FUV. Thus, we increased $\log\Lambda$ in that model from 3.6 to 4.0, which then adequately explained the fluxes in that bandpass. At photometric minimum, however, we found that the predicted flux was well down (by a factor of 5) from the GALEX data. While the nature of this discrepancy remains unclear, it is possible that the UV cyclotron emission region is not co-located with the optical accretion spot. If it were located closer to the pole, the accretion spot would just barely self eclipse, leaving a much larger emitting surface area and that could possibly explain this result.

7. Discussion

As UV data accumulate on Polars during low states of accretion, it is increasingly obvious that some areas emitting substantial UV flux remain on the white dwarf even during states of very low accretion when there is no evidence of a mass transfer stream. Studies of

Polars at random times (Ramsay et al. 2004; Araujo-Betancor et al. 2005) show that many Polars are in low states, implying they spend much of their lifetime in these states, but the length of these low states are not usually known and the data that do exist reveal the low states vary in length. For a few well-studied systems, the extra UV light over that of the white dwarf continuum is known as a function of time since the onset of the low state and is modelled with a hot spot. The study of AM Her (Gänsicke et al. 2006) with HST and FUSE for several months starting 200 days after it began a low state showed that the spot was about 10,000K cooler than its high state fitted value of 47,000K, but of a similar size as compared to a high state of accretion. There was also a slight change in latitude of the spot between the two states. These characteristics did not change during the 4 months of the low state. However, AM Her is known to have frequent high states of accretion which can heat up a spot and the derived accretion rate during low states is fairly high at $6 \times 10^{-12} M_{\odot} \text{ yr}^{-1}$. This value is about a factor of 10 below the typical mass accretion rate for a Polar in a high accretion state but a factor of 100 larger than a typical LARP (S05). The white dwarf temperature at 20,000K is close to the value of typical cataclysmic variables that are heated by long term accretion (Sion 1999, Townsley & Bildsten 2004).

Our UV (S06) and the X-ray (Sw07) study of EF Eri probe a longer and lower state of accretion compared to AM Her. The GALEX and X-ray data were obtained 7 and 5 yrs respectively into the low state that began in 1997 and has now reached 10 yrs in length. SW07 estimate the accretion luminosity during the low state as $2.4 \times 10^{30} \text{ erg s}^{-1}$, which corresponds to an accretion rate of about $3 \times 10^{-13} M_{\odot} \text{ yr}^{-1}$. The corresponding specific accretion rate of $0.01 \text{ g cm}^{-2} \text{ s}^{-1}$ puts EF Eri into the bombardment regime where there is no shock at the accretion column and there is only cyclotron cooling in the atmosphere of the white dwarf which result in the observed harmonics in the near-IR (Kuijpers & Pringle 1982; Woelk & Beuermann 1996; Wickramasinghe & Ferrario 2000). The resulting lower temperature of the white dwarf in EF Eri than in AM Her is consistent with low accretion values and long time intervals spent at low states.

MQ Dra is the most extreme case studied so far. It has one of the coolest white dwarfs and one of the lowest accretion rates ($6 \times 10^{-14} M_{\odot} \text{ yr}^{-1}$; S05) known among close binaries containing magnetic white dwarfs. It has never been seen in a high accretion state and the low white dwarf temperature and long orbital period indicate it may never have been in an active state. Thus, it is surprising that even in this regime, there is a significant UV source of light above that from a white dwarf that fits the optical continuum between cyclotron harmonics, and this source is highly variable during the orbit. If this UV source is from a heated area around the magnetic pole, the capture of the stellar wind from the secondary by the magnetic white dwarf must be able to produce a significant heating of the atmosphere for extended times. As noted by S05, Li et al. (1994;1995) determined that for fields near

50-100MG, the magnetic white dwarf can capture all of the stellar wind from the secondary, thus increasing the amount coming to the white dwarf. The figures in these papers suggest that the wind still is confined to a footprint near the magnetic pole(s). While the exact shape of a heated spot is not clear in this situation, it is reasonable that the heated area would be in the same location as the pole and in phase with the optical cyclotron emission (the low optical depth ensures the lowest harmonics are optically thin and hence the cyclotron is not beamed as in the optically thick case). In addition, the magnetic coupling between the two stars can lead to increased stellar activity (flares and coronal mass ejections) on the secondary, thus increasing the accretion rate sporadically and creating more heating (Howell et al. 2006). However, a simple hot spot is not an ideal fit to the observations as described above.

An alternate possibility is that the extra UV flux and modulation is caused by cyclotron harmonics in the UV. The greatest problem with this interpretation is that to have prominent harmonics in the UV requires a magnetic field > 200 MG. Possible harmonics are evident in the UV in AR UMa (Gänsicke et al. 2001) which is known to have a field of about 240 MG. However, recent modeling of the optical flux and polarization of EF Eri (Beuermann et al. 2007) shows that this system (as well as other Polars) has complex fields, with multipoles that could include fields up to 110MG. Recent success in modeling IR phase-resolved spectra of EF Eri (Campbell et al. 2008) was achieved with a two component cyclotron model. The extension of this type of model to the UV with a field of 115 MG can explain the amplitudes of the *GALEX* light curves for EF Eri. If MQ Dra has such a complex multipole field, then the optical cyclotron could be produced by fields near 60 MG and the UV cyclotron by the components near 200 MG. The correct interpretation could be resolved by time-resolved UV spectra which would reveal whether these cyclotron harmonics actually exist in the UV.

8. Conclusions

Our GALEX NUV and FUV light curves have revealed that the lowest accretion rate Polars, with no active stream accretion, still show large amplitude periodic UV variability with similar phasing and amplitude to the optical light curves. The extreme case of MQ Dra, with a long orbital period and a white dwarf of only 8000K, shows similar FUV variability to that of EF Eri, a Polar with extended low states but also a known high state of accretion in the past. The sequence of white dwarf temperatures appears to follow the accretion rates, with the lowest temperature white dwarfs existing in the systems with the lowest accretion, implying some long term heating effects even in these cases of wind-accretion. However, attempts to fit the UV light curves with a simple isothermal hot spot cannot adequately

describe the observations. While this simple type of spot can produce the amplitudes of the NUV and FUV modulation in EF Eri, it cannot reproduce the shape of the light curves well, implying distorted, multi-temperature spots or additional components. MQ Dra is harder to fit with a spot than EF Eri, as the similar amplitudes in NUV and FUV cannot be reproduced with a similar size spot at a given temperature.

Another explanation of the UV phasing and amplitudes might be possible using cyclotron harmonics, but only if the white dwarf has multipoles with fields extending above 200 MG. While we could adequately model optical phase-resolved spectroscopy of MQ Dra with a cyclotron model having $B = 59$ MG, $kT \simeq 2.0$ keV, and $\log\Lambda = 4.0$, both the observed motion of the harmonics and the morphological appearance of the spectra at cyclotron minimum and maximum defied our simplistic expectations. To explain these results in a consistent way would require a secondary that does not fill its Roche lobe, an accretion column that has a high magnetic co-latitude ($\beta = 45^\circ$), field lines that are tilted relative to the local normal, and an emitting region of the white dwarf that decreases by a factor of 6 from cyclotron maximum to minimum. The SED from the FUV to the K -band can be fit with an 8000 K WD, an M4 secondary normalized to the K -magnitude at photometric minimum and two cyclotron models (our derived optical cyclotron model and a second analogous cyclotron model with an equivalent peak flux in $n = 3$). This combination can reproduce the observed UV photometric variability, but at photometric minimum the UV cyclotron model must be scaled by an arbitrary value of 5 (possibly explained by moving the UV accretion spot closer to the rotation axis).

UV phase resolved spectra are needed to determine which model to pursue in more detail. The spectra would enable the temperature structure of a hot spot to be determined and reveal if cyclotron features from high fields are present. Further theoretical models of the atmospheric heating and cooling in the bombardment case of very low specific accretion would also help to determine the nature of the heated areas surrounding the magnetic poles at these low rates.

Support for this research was provided by NASA GALEX grant NNG05GG46G. We thank Hugh Harris for providing standard stars for the calibration of the optical data and Gary Schmidt for the use of his optical spectra of MQ Dra for the cyclotron model and for his comments on our models.

REFERENCES

Araujo-Betancor, S. et al. 2005, ApJ, 622, 589

- Bergeron, P., Wesemael, F. & Beauchamp, A. PASP, 107, 1047
- Beuermann, K., Stella, L. & Patterson, J., 1987, ApJ, 316, 360
- Beuermann, K., Euchner, F., Reinsch, K., Jordan, S. & Gänsicke, B. T. 2007, A&A, 463, 647
- Campbell, R. K., Harrison, T. E., Schwobe, A. & Howell, S. B. 2008, ApJ, 672, 531
- Claret, A. 2000a, A&A, 359, 289
- Claret, A. 2000b, A&A, 363, 1081
- Gänsicke, B. T., Long, K. S., Barstow, M. A. & Hubeny, I. 2006, ApJ, 639, 1039
- Gänsicke, B. T., Schmidt, G. D., Jordan, S. & Szkody, P. 2001, ApJ, 555, 380
- Harrison, T. E., Howell, S. B., Szkody, P. & Cordova, F. A. 2005, ApJ, 632, L123
- Howell, S. B., et al. 2006, ApJ, 652, 709
- Hubeny, I. 1988, Comp. Phys. Comm., 52, 103
- Hubeny, I., Lanz, T., & Jeffery, C. S. 1994, in Newsletter on Analysis of Astronomical Spectra No. 20, ed. C. S. Jeffery (CCP7; St. Andrews: St. Andrews Univ.), 30
- Kuijpers, J. & Pringle, J. E. 1982, A&A, 114, L4
- Li, J., Wickramasinghe, D. T., & Wu, K. W. 1995, MNRAS, 276, 255
- Li, J., Wu, K. W. & Wickramasinghe, D. T. 1994, MNRAS, 268, 61
- Linnell, A. P. & Hubeny, I. 1996, ApJ, 471, 958
- Martin, D. C. et al. 2005, ApJ, 619, L1
- Nordlund, A. & Vaz, L. P. R. 1990, A&A, 228, 231
- Ramsay, G. et al. 2004, MNRAS, 350, 1373
- Schmidt, G. D. et al. 1996, ApJ, 473, 483
- Schmidt, G. D. et al. 2005, ApJ, 630, 1037 (S05)
- Schwobe, A. D. 1990, Reviews in Modern Astronomy, 3, 44
- Schwobe, A. D. et al. 2002, in ASP Conf. Vol 261, The Physics of Cataclysmic Variables and Related Objects, ed. B. T. Gänsicke, K. Beuermann, & K. Reinsch (San Francisco:ASP), 102
- Schwobe, A. D., Staude, A., Koester, D. & Vogel, J. 2007, aap, 469, 1027 (Sw07)
- Sion, E. M. 1999, PASP, 111, 532
- Szkody, P. et al. 2003, ApJ, 583, 902 (S03)

Szkody, P. et al. 2004, *AJ*, 128, 2443

Szkody, P. et al. 2006, *ApJ*, 646, L147 (S06)

Townsley, D. M. & Bildsten, L. 2004, *ApJ*, 600, 390

Wickramasinghe, D. T. & Ferrario, L. 2000, *PASP*, 112, 873

Woelk, U. & Beuermann, K. 1996, *A&A*, 306, 232

Table 1. Summary of Observations

Date	Time	Data
20050607	04:48-19:52	GALEX NUV 10 visits
20050723	11:53-12:13	GALEX NUV 1 visit
20060715	16:40-17:04	GALEX NUV,FUV 1 visit
20060716	01:08-02:55	GALEX NUV,FUV 2 visits
20060716	07:27-09:30	GALEX NUV,FUV 2 visits
20060716	17:20-21:02	GALEX NUV,FUV 3 visits
20060717	01:46-03:35	GALEX NUV,FUV 2 visits
20060722	03:13-03:33	GALEX NUV,FUV 1 visit

Table 2. Roche-filling Factor vs Inclination

$R/R_{contact}$	i°
1.00	35
0.94	40
0.90	47
0.86	54
0.82	65

Table 3. MQ Dra Model Parameters

Parameter	i=60°	i=35°
WD T_{eff}	8000K	8000K
WD mass	0.6M _⊙	0.6M _⊙
WD radius	0.012R _⊙	0.012R _⊙
WD log g	8.0	8.0
Spot T_{eff}	20,000K	24,000K
Spot latitude	73°	65°
Spot ang rad	5° (FUV)	3.5° (FUV)
Spot ang rad	12° (NUV)	14° (NUV)

Table 4. EF Eri Model Parameters

Parameter	Value
WD T_{eff}	9500K
WD mass	$0.6M_{\odot}$
WD radius	$0.012R_{\odot}$
WD log g	8.0
Orbit i	45°
Spot T_{eff}	24,000K
Spot latitude	60°
Spot ang rad	5.5°

Table 5. Comparison of EF Eri Models

Parameter	Sw07	This work
WD T(K)	9750	9500
Spot T (K)	18,500	24,000
Inclination ($^{\circ}$)	60	45
Spot Ang radius ($^{\circ}$)	24	5.5
Spot Latitude ($^{\circ}$)	77.5	60

Table 6. Cyclotron Modeling Parameters for MQ Dra

Spectrum	Phase	B (MG)	T (keV)	Θ	$Log(\Lambda)$
1	0.67	59.0	2.0	70.0	4.1
2	0.73	59.0	1.6	68.0	4.1
3	0.82	59.0	1.6	65.0	3.8
4	0.89	59.0	1.8	63.0	3.6
5	0.95	59.0	1.8	61.0	3.6
6	0.02	59.0	1.8	63.0	3.6
7	0.09	59.0	1.8	65.0	3.6
8	0.16	59.0	1.8	67.0	3.7
9	0.23	59.0	1.8	70.0	3.7
10	0.30	59.0	1.9	72.0	3.7
11	0.36	59.0	2.0	74.0	3.9
12	0.43	59.0	2.0	76.0	3.9
13	0.50	59.0	2.0	74.0	3.9
14	0.57	59.0	2.0	72.0	3.9

Table 7. Relation of Column Height to i and β

h_{col} (R_{WD})	$i + \beta$	i
0.01	97.5°	52.5°
0.02	100.5°	56.5°
0.03	102.9°	57.9°
0.04	104.8°	59.8°
0.05	106.5°	61.5°

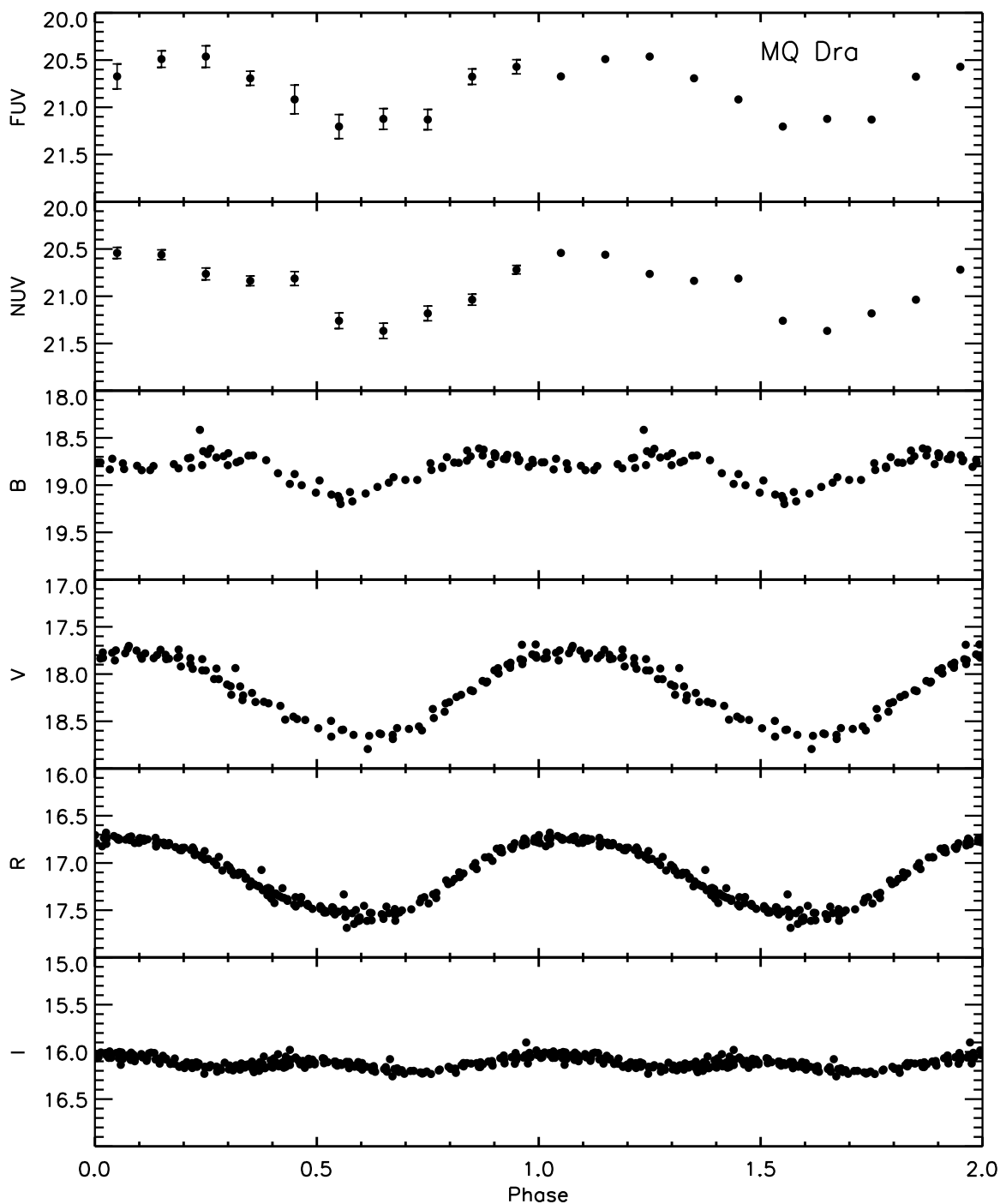


Fig. 1.— GALEX FUV and NUV and optical B,V,R,I filter light curves as a function of phase (phase 0 is cyclotron max and inferior conjunction of secondary). Light curves are repeated from phases 1.0 to 2.0, with error bars shown only for the first cycle. Error bars for the optical data are smaller than the points.

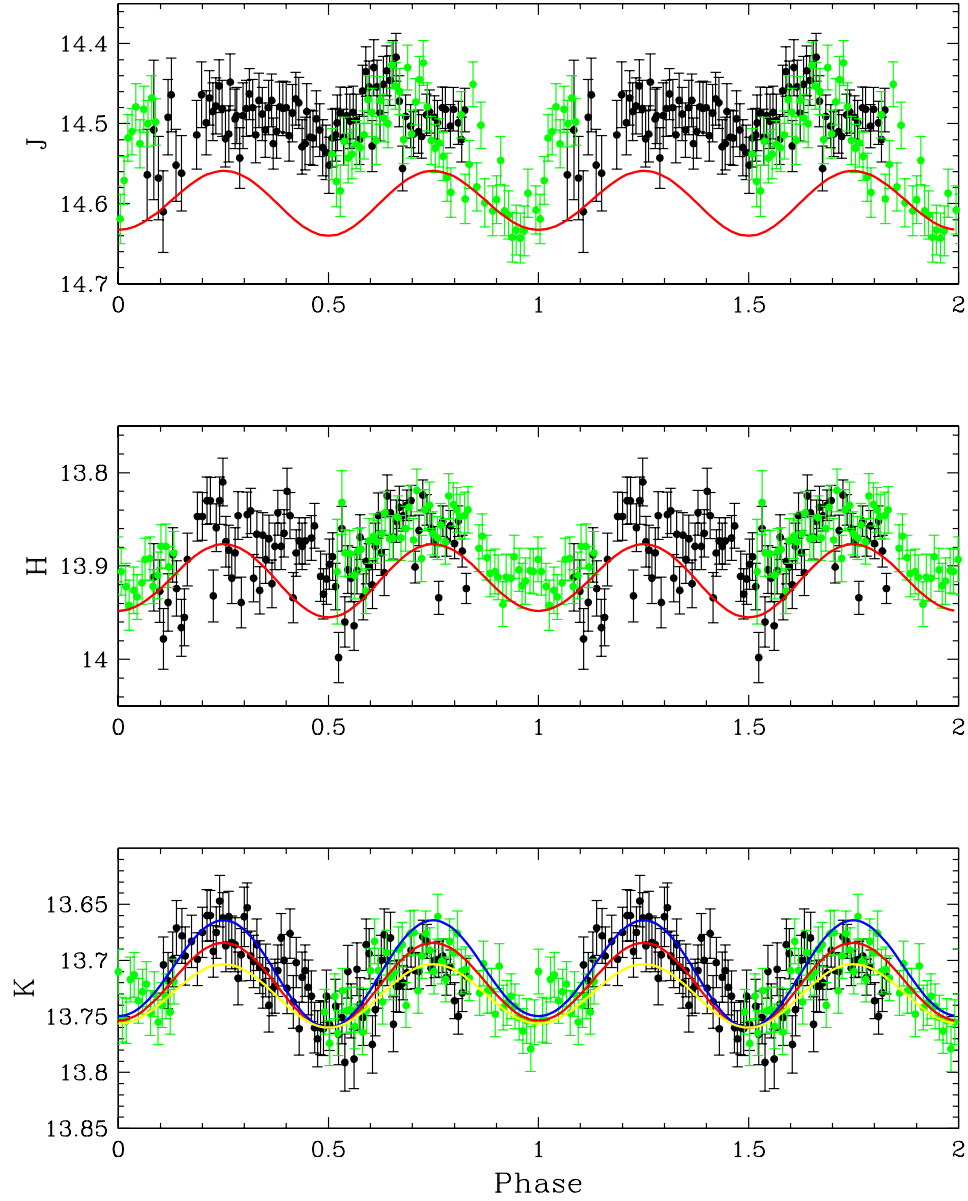


Fig. 2.— J , H , K light curves of MQ Dra (green is May 28 and black is May 29) fit with a model of an M4 secondary filling its Roche lobe and an 8000K white dwarf. Inclinations of 40, 35 and 30° are shown as blue, red and yellow lines respectively; for clarity, only the best fitting 35° fit is shown for J , H .

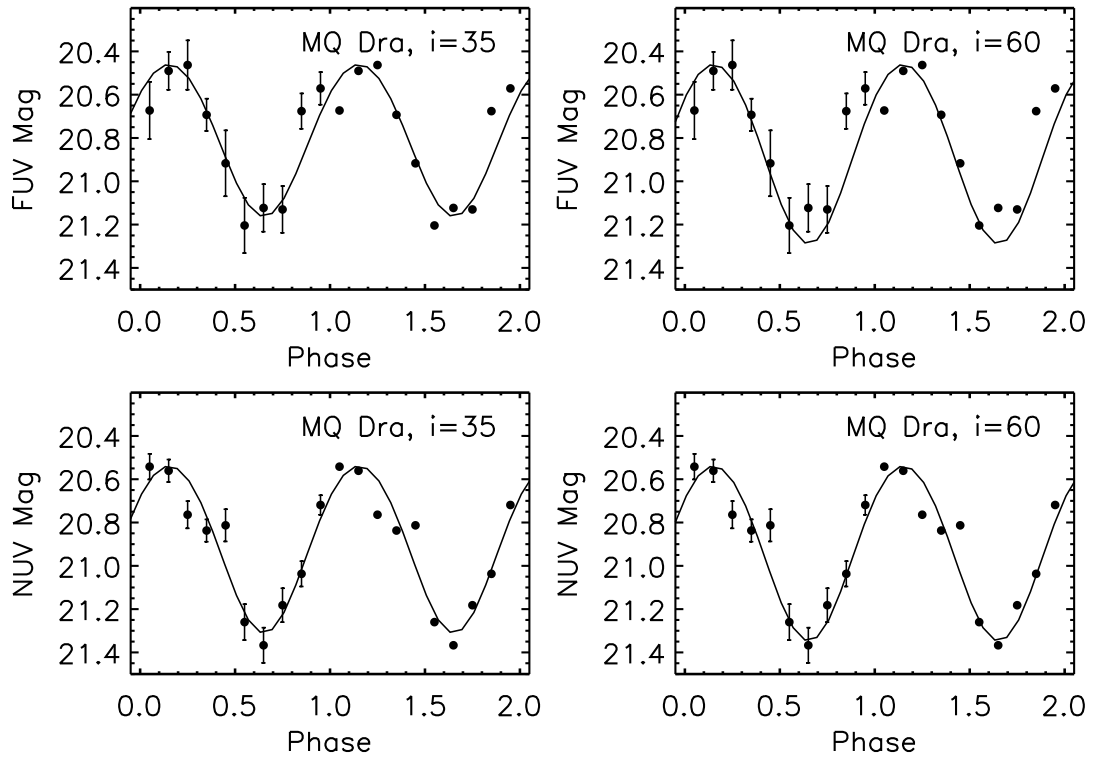


Fig. 3.— Spot Model fits from Table 3 for the GALEX FUV (top) and NUV (bottom) light curves of MQ Dra for inclinations of 35° (left) and 60° (right).

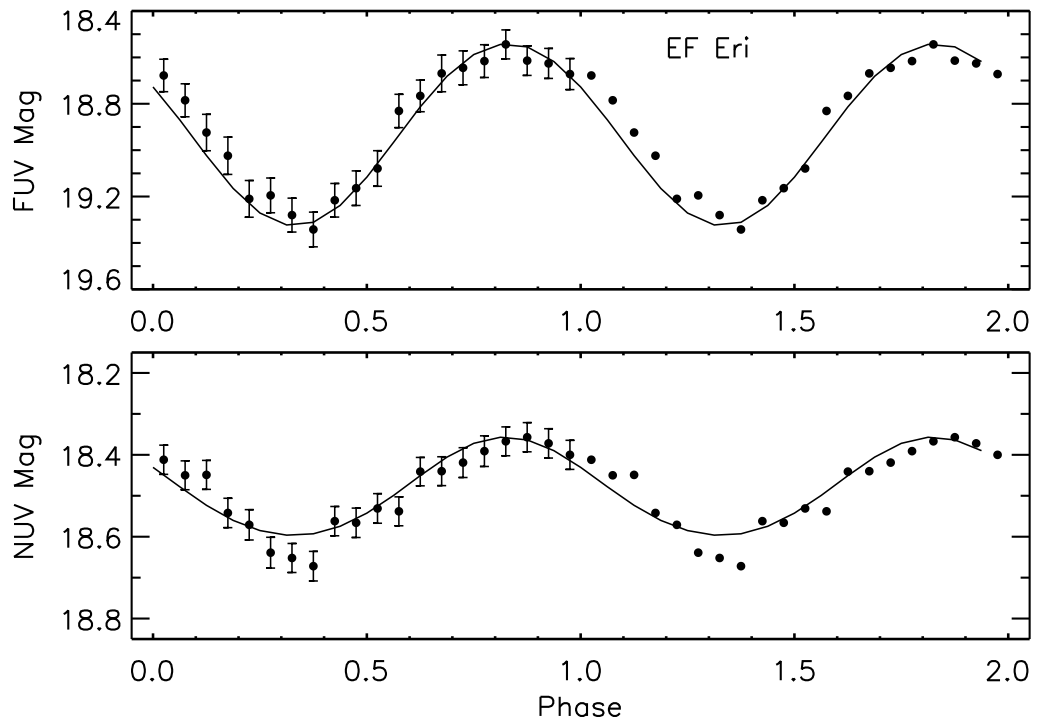


Fig. 4.— Model fit for EF Eri with a 24,000K spot at 60° latitude and 5.5° radius on a 9500K white dwarf.

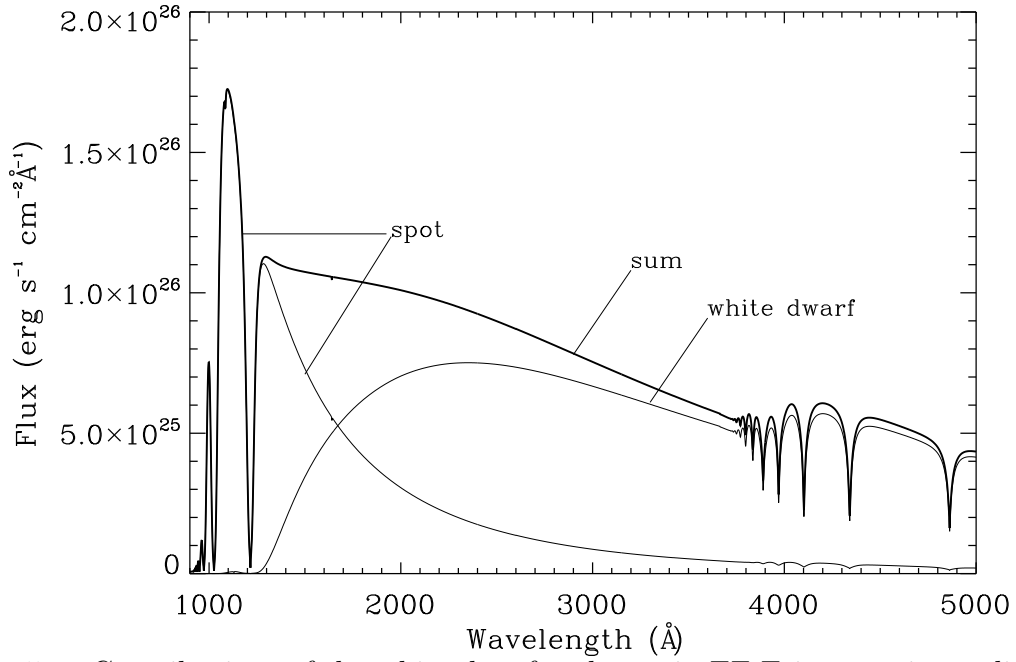


Fig. 5.— Contributions of the white dwarf and spot in EF Eri at maximum light during the orbit.

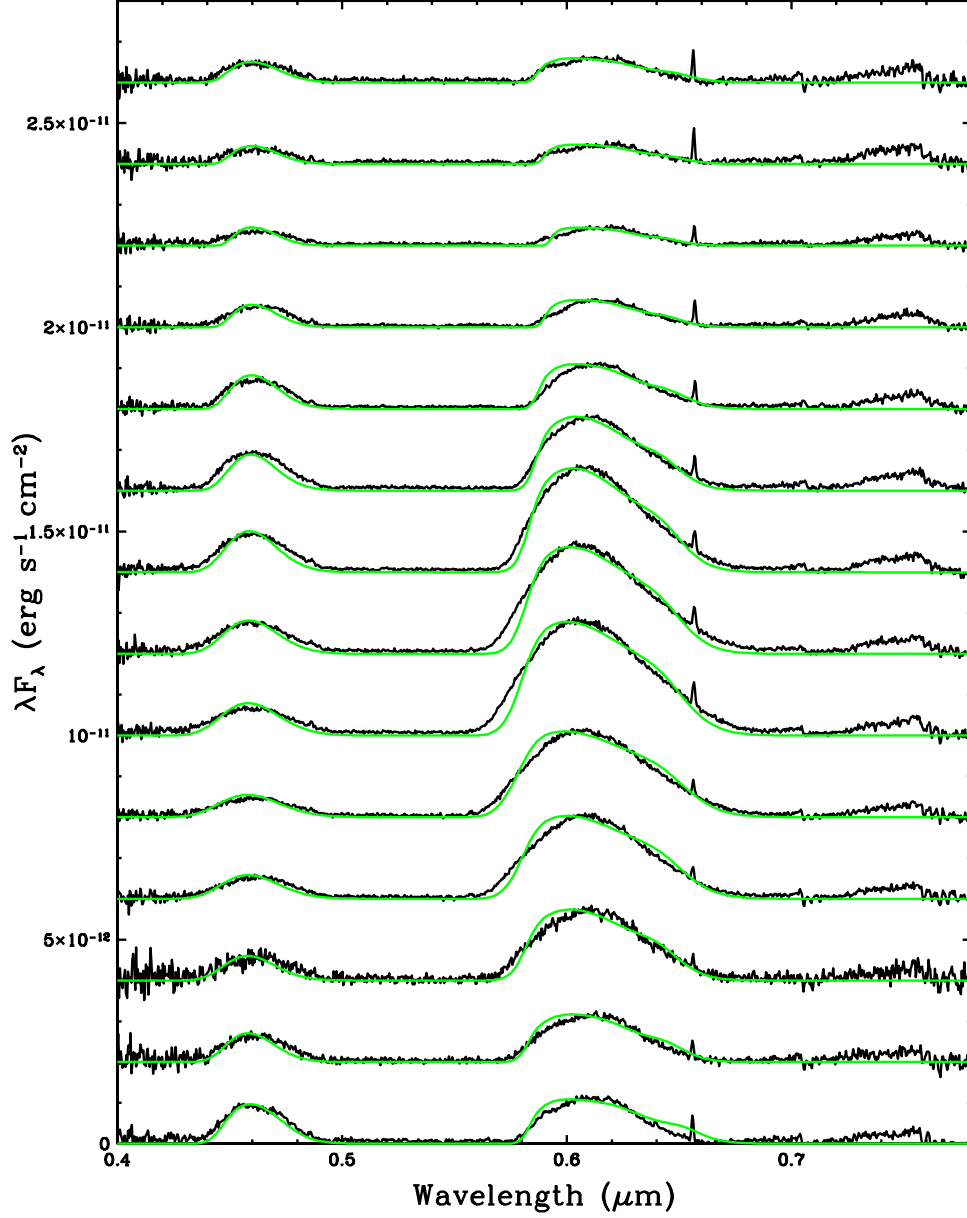


Fig. 6.— Phase-resolved spectra of MQ Dra, data (in black) from S05 are stacked with a constant increment of $2.0 \times 10^{-12} \text{ erg s}^{-1} \text{ cm}^{-2}$. The best fit cyclotron models (in green) are fit over the cyclotron models, with spectrum 1 at bottom and 14 at top from Table 6.

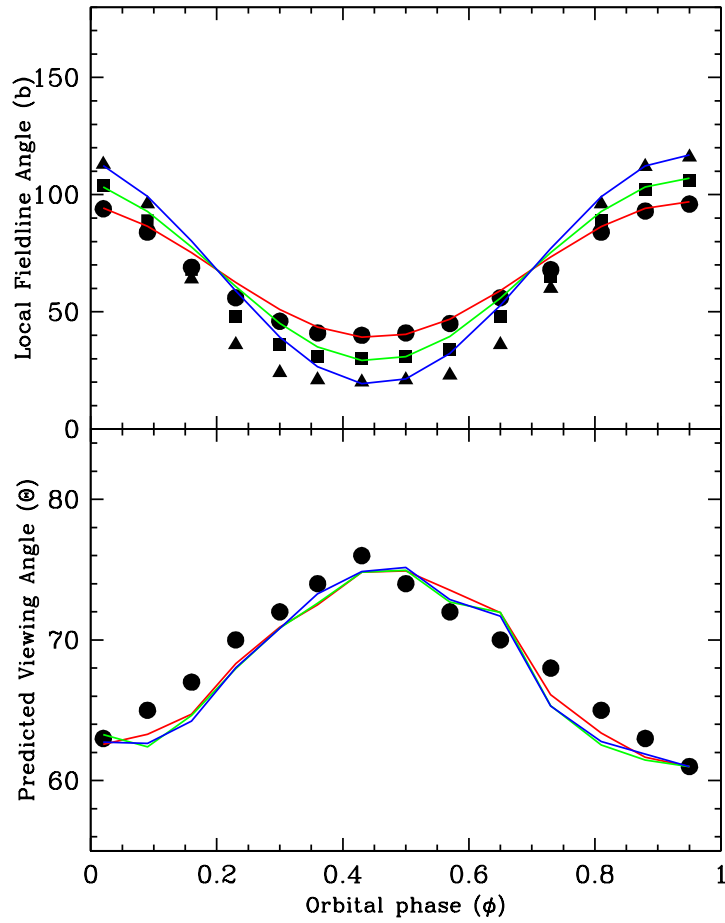


Fig. 7.— (top) The change in the local field angle for three orbital inclinations 35° (circles), 45° (squares), 55° (triangles), that reproduced the observed viewing angle variation (bottom panel, circles). The colored lines shown in the top panel to guide the eye are reproduced in the bottom panel to demonstrate that this interpretation can reproduce the observed variation in viewing angle.

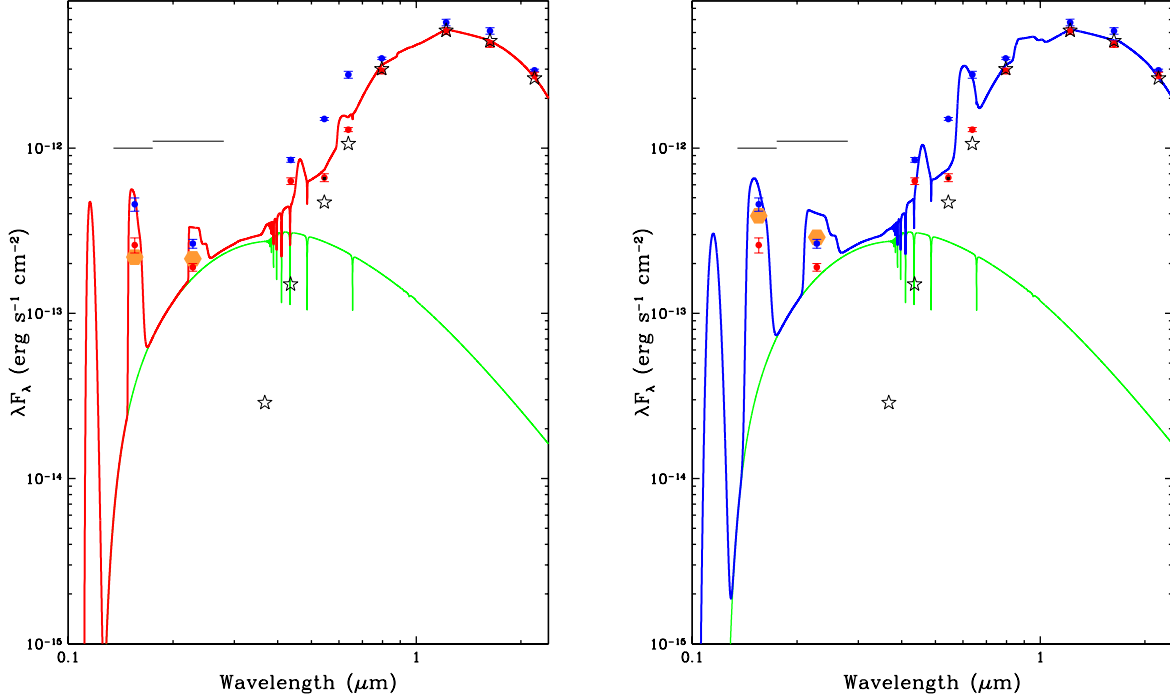


Fig. 8.— (a) Cyclotron model SED of MQ Dra at photometric minimum ($\phi = 0.65$). Horizontal lines are GALEX bandpasses, points are UV optical and IR photometric observations (red are photometric min, blue are photometric max), and the green line is the spectrum of an 8000K WD, normalized to $\simeq 20\%$ below the NUV photometric point. Stars are an M4 spectrum normalized to the K -band point. Our cyclotron model at photometric minimum and an analogous UV model, with $B = 235$ MG, are added in normalized so that the peak-value of F_λ in the $n = 3$ harmonics of both the optical and UV cyclotron models are identical, but the UV model is scaled up by a factor of five (see text for details). The overall fit is plotted in red. Orange hexagons are the NUV and FUV photometry implied by our models assuming the NUV and FUV transmissions. (b) Similar but for photometric max, with the final composite model now shown in blue. No scaling to account for the UV fluxes is used in this case.